



Abschlussarbeit im Masterstudiengang Physik der
Kondensierten Materie

Entwicklung eines diagonalen isometrischen Tensor Netzwerk Algorithmus

Development of a diagonal isometric Tensor Network Algorithm

Benjamin Sappler

18. April 2024

Erstgutachter (Themensteller): Prof. F. Pollmann
Zweitgutachter: Unknown

I hereby declare that this thesis is entirely the result of my own work except where otherwise indicated. I have only used the resources given in the list of references.

Munich, 99.99.2099

Benjamin Sappler

Abstract

The numerical simulation of strongly interacting quantum many-body systems is a challenging problem. In the last decades, Tensor Networks have emerged as the standard method for tackling this problem in one dimensional systems in the form of Matrix Product States (MPS). Tensor Networks have also been generalized for the highly relevant problem of two and more spatial dimensions. However, these so-called Projected Entangled Pair States (PEPS) are typically plagued by high computational complexity or drastic approximations. Recently, a new class of Tensor Networks, called isometric Tensor Networks, have been proposed for the simulation of two-dimensional quantum systems. This new class of Tensor Networks can be understood as a generalization of the one-dimensional Matrix Product States to higher dimensions. While isometric Tensor Networks generally capture only a subspace of the total Hilbert space, there are already promising results. In this work, we develop a new class of isometric Tensor Networks that has some key differences to the existing one. We show first numerical results for finding ground states of the Transverse Field Ising model.

Zusammenfassung



Contents

1	Introduction	1
2	Tensors and Tensor Networks	3
2.1	Conventions and Notation	3
2.2	Tensor Decompositions	7
2.3	Isometric Tensor Networks	8
2.4	Matrix Product States (MPS)	9
2.5	Isometric Tensor Product States in 2D	15
3	diagonal isometric Tensor Product States (disoDTPS)	21
3.1	Network Structure	21
3.2	Yang-Baxter Move	24
3.3	Time Evolving Block Decimation (TEBD)	27
4	Toric Code: An exactly representable Model	29
5	Transverse Field Ising Model: Ground State Search and Time Evolution	31
A	Riemannian Optimization of Isometries	33
A.1	The complex Stiefel manifold	33
A.2	Gradients, retractions, and vector transport	34
A.3	Conjugate Gradients	35
A.4	Trust Region Method	35
B	Initialization of the Disentangling Unitary	37
	Bibliography	39

Chapter 1

Introduction

Chapter 2

Tensors and Tensor Networks

In the following, a brief introduction to tensors, tensor networks, and tensor network algorithms is given. We start by defining the conventions and notation used in this thesis in section 2.1. In section 2.2, we introduce important tensor decompositions that are used extensively in tensor network algorithms. In section 2.3, we define isometric tensor networks and discuss their properties. Lastly, we give examples for physical states being represented in terms of isometric tensor networks, namely the popular Matrix Product States (MPS) in section 2.4 and the recently developed isometric tensor product states in 2D (isoTPS) in section 2.5.

2.1 Conventions and Notation

Tensors

For the purpose of this thesis we define a *tensor* T of rank n as an n -dimensional array of complex numbers

$$T \in \mathbb{C}^{\chi_1 \times \chi_2 \times \dots \times \chi_n}, \quad \chi_i \in \{1, 2, \dots\}$$

with entries

$$T_{i_1 i_2 \dots i_n} \in \mathbb{C}, \quad i_j \in \{1, 2, \dots, \chi_j\}.$$

For example, a rank-0 tensor is a scalar, a rank-1 tensor is a vector, and a tensor of rank-2 is a matrix.

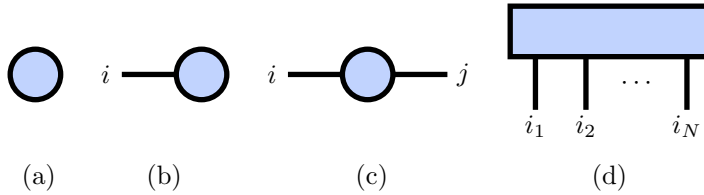


Figure 2.1: Tensors of different ranks are shown in diagrammatic notation. (a) A scalar, (b) a vector, (c) a matrix, (d) a general tensor of rank N .

An *index contraction* between two or more tensors is the linear operation that is performed by summing over a given set of indices. For example, the matrix product of two matrices $A \in \mathbb{C}^{\chi_1 \times \chi_2}$ and $B \in \mathbb{C}^{\chi_2 \times \chi_3}$ can be written as the index contraction

$$C_{ij} = \sum_{\alpha=1}^{\chi_2} A_{i\alpha} B_{\alpha j}. \quad (2.1)$$

A more involved example is the index contraction of two rank-3 tensors $A \in \mathbb{C}^{\chi_1 \times \chi_2 \times \chi_3}$, $B \in \mathbb{C}^{\chi_2 \times \chi_4 \times \chi_5}$ and one rank-4 tensor $C \in \mathbb{C}^{\chi_3 \times \chi_5 \times \chi_6 \times \chi_7}$, where we contract along the indices with dimension χ_2 , χ_3 and χ_5 . The result is a rank-4 tensor $D \in \mathbb{C}^{\chi_1 \times \chi_4 \times \chi_6 \times \chi_7}$:

$$D_{ijkl} = \sum_{\alpha=1}^{\chi_2} \sum_{\beta=1}^{\chi_3} \sum_{\gamma=1}^{\chi_5} A_{i\alpha\beta} B_{\alpha j\gamma} C_{\beta\gamma kl}. \quad (2.2)$$

More generally, given a rank- $(n + f)$ tensor $A \in \mathbb{C}^{\chi_1 \times \dots \times \chi_n \times \xi_1 \times \dots \times \xi_f}$ and a rank- $(m + f)$ tensor $B \in \mathbb{C}^{\lambda_1 \times \dots \times \lambda_m \times \xi_1 \times \dots \times \xi_f}$, the result of contracting A and B along the last f indices produces a new rank- $(m + n)$ tensor $C \in \mathbb{C}^{\chi_1 \times \dots \times \chi_n \times \lambda_1 \times \dots \times \lambda_m}$ as

$$C_{i_1 \dots i_n j_1 \dots j_m} := \sum_{\mu_1=1}^{\xi_1} \dots \sum_{\mu_f=1}^{\xi_f} A_{i_1 \dots i_n \mu_1 \dots \mu_f} B_{j_1 \dots j_m \mu_1 \dots \mu_f}. \quad (2.3)$$

Contractions over arbitrary indices can be reformulated as contractions over the last f indices by transposing the tensors. Contractions over more than two tensors can be decomposed into successive contractions of two tensors. Because tensor contractions are linear, the order in which tensors are contracted doesn't change the result. However, the computational complexity does in general depend on the order of contractions and can thus be minimized by choosing the optimal contraction order.

By counting the number of multiplications and additions that are necessary to perform the tensor contraction (2.3), the computational complexity can be determined as

$$\mathcal{O} \left(\prod_{\mu=1}^n \chi_{\mu} \prod_{\mu=1}^m \lambda_{\mu} \prod_{\mu=1}^f \xi_{\mu} \right).$$

Tensor Networks

A *tensor network* is defined as a collection of tensors that are contracted in a specified way. It is convenient to introduce a diagrammatic notation, where tensors are drawn as shapes and tensor indices are represented by lines emerging from these

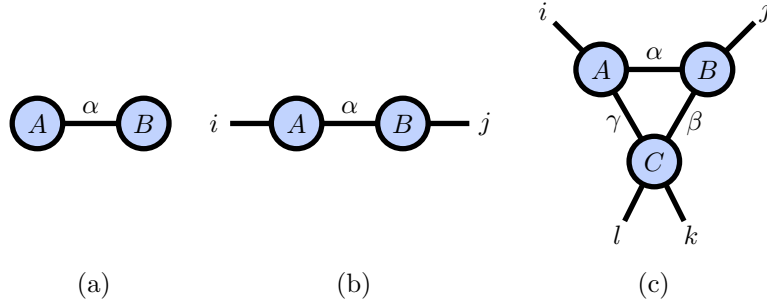


Figure 2.2: Tensor networks in diagrammatic notation. (a) Scalar product (2.4). (b) Matrix product (2.1). (c) More involved network consisting of three tensors (2.2).

shapes. To relate this diagrammatic notation to equations, one often decorates each line with the corresponding index i_j . A scalar, vector, matrix, and a general rank- n tensor are visualized in this notation in figure 2.1. Index contractions are depicted diagrammatically by connecting the lines corresponding to contracted indices. Lines connecting two tensors are sometimes called *bonds*, while indices not used in contractions are called *open indices*. The *bond dimension* χ_i denotes the number of different values an index i can take. It is often more convenient to discuss tensor network algorithms in terms of diagrams than in terms of equations. Two simple tensor networks are the scalar-product of two vectors

$$c = \sum_{\alpha=1}^{\chi} A_{\alpha} B_{\alpha} \quad (2.4)$$

and the matrix product (2.1). Both networks are shown as diagrams in figure 2.2(a) and 2.2(b) respectively. 2.2(c) depicts the more involved tensor network (2.2).

Isometries

Given two normed vector spaces V_1 and V_2 with $\dim(V_1) = m$, $\dim(V_2) = n$, $m \leq n$, an *isometry* (sometimes also called *semi-unitary*) is a linear, norm-preserving map $W : V_1 \rightarrow V_2$ from the smaller to the larger vector space. Each isometry can be represented by a $n \times m$ matrix W fulfilling the *isometry condition*

$$W^{\dagger}W = \mathbb{1}, \quad WW^{\dagger} = \mathbb{P}, \quad (2.5)$$

where $\mathbb{P} = \mathbb{P}^2$ is a projection. If $m = n$, it holds $\mathbb{P} = \mathbb{1}$ and W is a *unitary map*. An isometry tensor is a tensor that through grouping of indices and reshaping (i.e. matricization) becomes an isometry. In tensor network diagrams, we draw isometries by decorating lines with arrows. Following the convention of [1, 2], we denote the

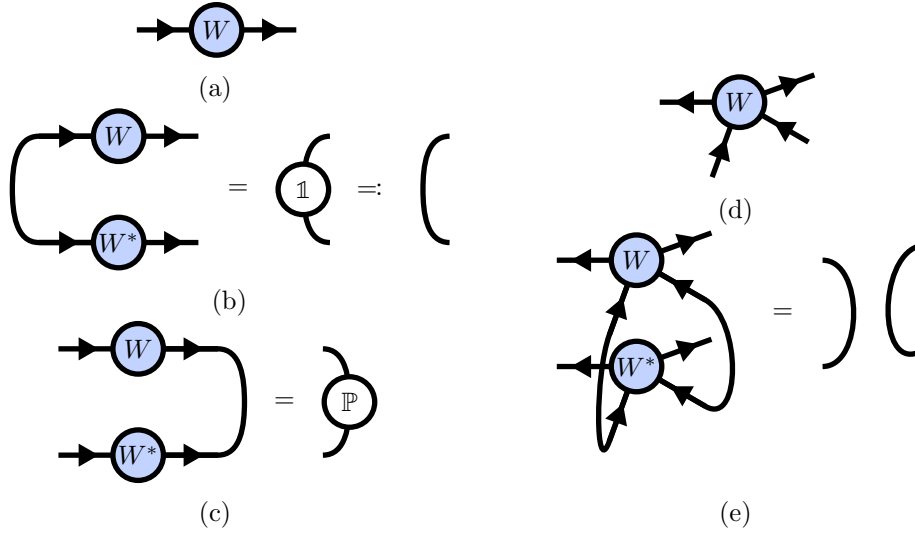


Figure 2.3: Isometric and unitary tensors are drawn by decorating indices with arrows. (a) diagrammatic notation of an isometric matrix (b) (c) The isometry condition (2.5) is depicted diagrammatically. (d) Isometric tensors of higher rank must fulfill the isometry condition by grouping of indices.

indices belonging to the larger vector space by incoming arrows and the indices belonging to the smaller vector space by outgoing arrows. Unitary tensors are decorated with bidirectional arrows on all indices, where the grouping must be inferred from the context. Ordinary tensors are drawn without arrows. Tensor diagrams for isometric and unitary tensors are shown in figure 2.3.

We lastly introduce an inner product for rank- n tensors $A, B \in \mathbb{C}^{\chi_1 \times \dots \times \chi_n}$, the *Frobenius inner product*

$$\langle A, B \rangle_F := \sum_{\mu_1=1}^{\chi_1} \dots \sum_{\mu_n=1}^{\chi_n} A_{\mu_1 \dots \mu_n}^* B_{\mu_1 \dots \mu_n} = \text{Tr} \left(A^\dagger B \right), \quad (2.6)$$

where the last equality holds only if $n = 2$. The Frobenius inner product induces a norm, the *Frobenius norm*

$$\|A\|_F = \sqrt{\langle A, A \rangle_F},$$

which can be used to define a measure of distance $\|A - B\|_F$ between tensors A and B .

2.2 Tensor Decompositions

There are three decompositions that are used extensively in this thesis: The QR-decomposition, the Singular Value Decomposition, and the Polar Decomposition. All three decompositions are matrix decompositions but can be applied to tensors as well by first grouping indices and reshaping to a matrix, applying the decomposition, and reshaping the result back to the original bond dimensions.

The *reduced QR-decomposition* of a matrix $A \in \mathbb{C}^{n \times m}$ is the decomposition

$$A = QR, \quad (2.7)$$

where $Q \in \mathbb{C}^{n \times k}$ is an isometry, $R \in \mathbb{C}^{k \times m}$ is an upper triangular matrix and $k := \min(n, m)$. The computational complexity of the QR decomposition scales as

$$\mathcal{O}(n \cdot m \cdot \min(n, m)). \quad (2.8)$$

A diagrammatic depiction of the QR decomposition (2.7) is drawn in figure 2.4(a). The *Singular Value Decomposition* (SVD) of a matrix $A \in \mathbb{C}^{n \times m}$ is the decomposition

$$A = USV^\dagger, \quad (2.9)$$

where $U \in \mathbb{C}^{n \times k}$ and $V \in \mathbb{C}^{m \times k}$ are isometries, $S \in \mathbb{R}^{k \times k}$ is a diagonal real matrix of *singular values*, and $k := \min(n, m)$. The computational complexity of the SVD is the same as for the QR decomposition (2.8). However, while the scaling is the same, the prefactors are lower for the QR decomposition in most implementations, meaning that the QR decomposition is faster in practice. Moreover, in contrast to the SVD, the QR decomposition allows for highly efficient implementations on graphics processing units (GPUs), which enables decompositions of large matrices to be carried out significantly faster and more power efficiently. Thus, whenever the singular values are not needed, the QR decomposition is preferred over the SVD. Figure 2.4 shows a tensor network diagram of the SVD (2.9).

An important property of the SVD is that it can be used to approximate a matrix A by a matrix \tilde{A} of lower rank $\chi < \min(m, n)$. This *truncated SVD* can be performed by keeping only the largest $\chi < k$ singular values and omitting the corresponding columns of U and V :

$$A \approx \tilde{A} = \tilde{U} \tilde{S} \tilde{V},$$

with isometries $\tilde{U} \in \mathbb{C}^{n \times \chi}$, $\tilde{V} \in \mathbb{C}^{m \times \chi}$ and real diagonal matrix $\tilde{S} \in \mathbb{C}^{\chi \times \chi}$. It can be shown [3] that the truncated SVD minimizes the distance $\|A - \tilde{A}\|_F$ between A and \tilde{A} under the constraint $\text{rank}(\tilde{A}) = \chi$. The truncated SVD is frequently used in tensor network algorithms to truncate tensors to a maximum bond dimension χ_{\max} . The *polar decomposition* of a matrix $A \in \mathbb{C}^{n \times m}$ is the decomposition

$$A = WP, \quad (2.10)$$

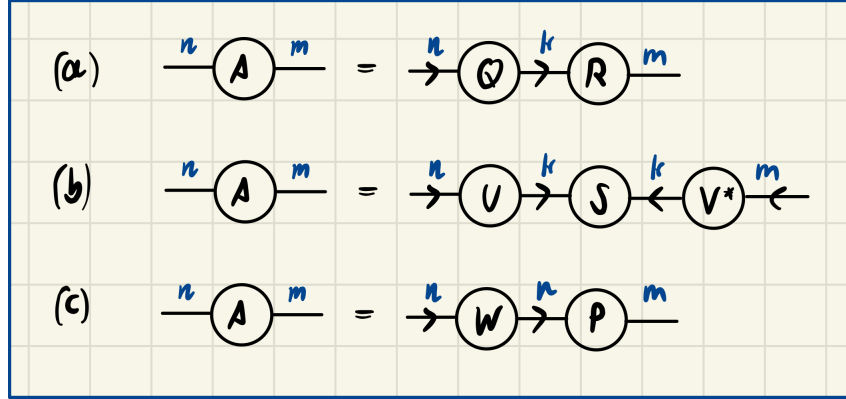


Figure 2.4: Different tensor decompositions are shown in tensor network diagram notation. The indices are decorated with bond dimensions. (a) QR decomposition (2.7). (b) Singular Value Decomposition (2.9). (c) Polar decomposition (2.10).

where $W \in \mathbb{C}^{m \times n}$ is an isometry and $P \in \mathbb{C}^{n \times n}$ is positive-definite and hermitean. The polar decomposition is related to the SVD $A = USV$ by

$$W = UV^\dagger, \quad P = VSV^\dagger.$$

The computational complexity of the polar decomposition is the same as for the QR decomposition and SVD (2.8). The polar decomposition (2.10) is depicted diagrammatically in figure 2.4. One can show that the W factor of the polar decomposition minimizes the distance $\|A - W\|_F$. Thus, the polar decomposition is often used in isometric tensor network algorithms to "isometrize" tensors.

2.3 Isometric Tensor Networks

An isometric tensor network is a tensor network whose diagrams bonds can be consistently assigned with arrows. In particular we will look at finite tensor networks where the arrows do not form any loops. In such networks, all arrows point to a single tensor, the *orthogonality center*. Such networks have the very useful property, that the error of local approximations around the orthogonality center can be computed locally (without contracting the full network). Let \mathcal{N} be the tensor that is the result of contracting the full network, and let \mathcal{M} be the tensor resulting from the contraction of a subregion of the network around the orthogonality center, where all arrows in the tensor network diagram point towards \mathcal{M} (see figure 2.5(a) for an example in tensor diagram notation). Let us now approximate the sub-network \mathcal{M} by a different sub-network \mathcal{M}' , which changes the contraction of the full network to

\mathcal{N}' (see 2.5(b)). We can compute the error ε of this approximation as

$$\begin{aligned}
 \varepsilon^2 &= \|\mathcal{N} - \mathcal{N}'\|_{\text{F}}^2 \\
 &= \langle \mathcal{N} - \mathcal{N}', \mathcal{N} - \mathcal{N}' \rangle_{\text{F}} \\
 &= \|\mathcal{N}\|_{\text{F}}^2 + \|\mathcal{N}'\|_{\text{F}}^2 - 2 \operatorname{Re} \langle \mathcal{N}, \mathcal{N}' \rangle_{\text{F}} \\
 &= \|\mathcal{M}\|_{\text{F}}^2 + \|\mathcal{M}'\|_{\text{F}}^2 - 2 \operatorname{Re} \langle \mathcal{M}, \mathcal{M}' \rangle_{\text{F}} \\
 &= \|\mathcal{M} - \mathcal{M}'\|_{\text{F}}^2,
 \end{aligned}$$

where in the fourth step we used the fact that all tensors outside of the sub-network satisfy the isometry condition. As an example, the contraction of $\operatorname{Tr}(\mathcal{N}\mathcal{N}^\dagger)$ is shown in figure 2.5(c). As one can see, the computation of the error reduces to a contraction of the local sub-networks. This greatly simplifies the computation of optimal approximations of tensors especially for large networks, because the full network doesn't need to be contracted. As will become clear in the next section, when the tensor network represents a quantum state, this also makes it very easy to compute local expectation values, because the computation of the overlap of the wavefunction can be simplified to a contraction of a local environment around the orthogonality center. Additionally, approximations made by the truncated SVD 2.2 and the isometrization using the polar decomposition 2.10 are, when performed at the orthogonality center, globally optimal for isometric tensor networks, instead of only locally optimal for non-isometric tensor networks.

2.4 Matrix Product States (MPS)

The Density Matrix Renormalization Group (DMRG) algorithm, which was subsequently understood as a variational method over the class of Matrix Product States (MPS), has developed to be the de-facto standard for the numerical simulation of one-dimensional quantum systems. The success of this method is due to the remarkable ability of MPS to capture the area-law entanglement characteristics of ground states of gapped Hamiltonians. Additionally, due to the elegant diagrammatic notation for tensor networks, new algorithms can be developed and discussed efficiently and intuitively. Applications of MPS include finding ground and thermal states, real and imaginary time evolution, and the computation of dynamical properties of lattice Hamiltonians. In the following we give a brief introduction to MPS, for a more in-depth discussion see [4–6]. The state of a quantum many-body system can be written as

$$|\Psi\rangle = \sum_{i_1=1}^{d_1} \sum_{i_2=1}^{d_2} \cdots \sum_{i_N=1}^{d_N} \Psi_{i_1 i_2 \dots i_N} |i_1\rangle \otimes |i_2\rangle \otimes \cdots \otimes |i_N\rangle.$$

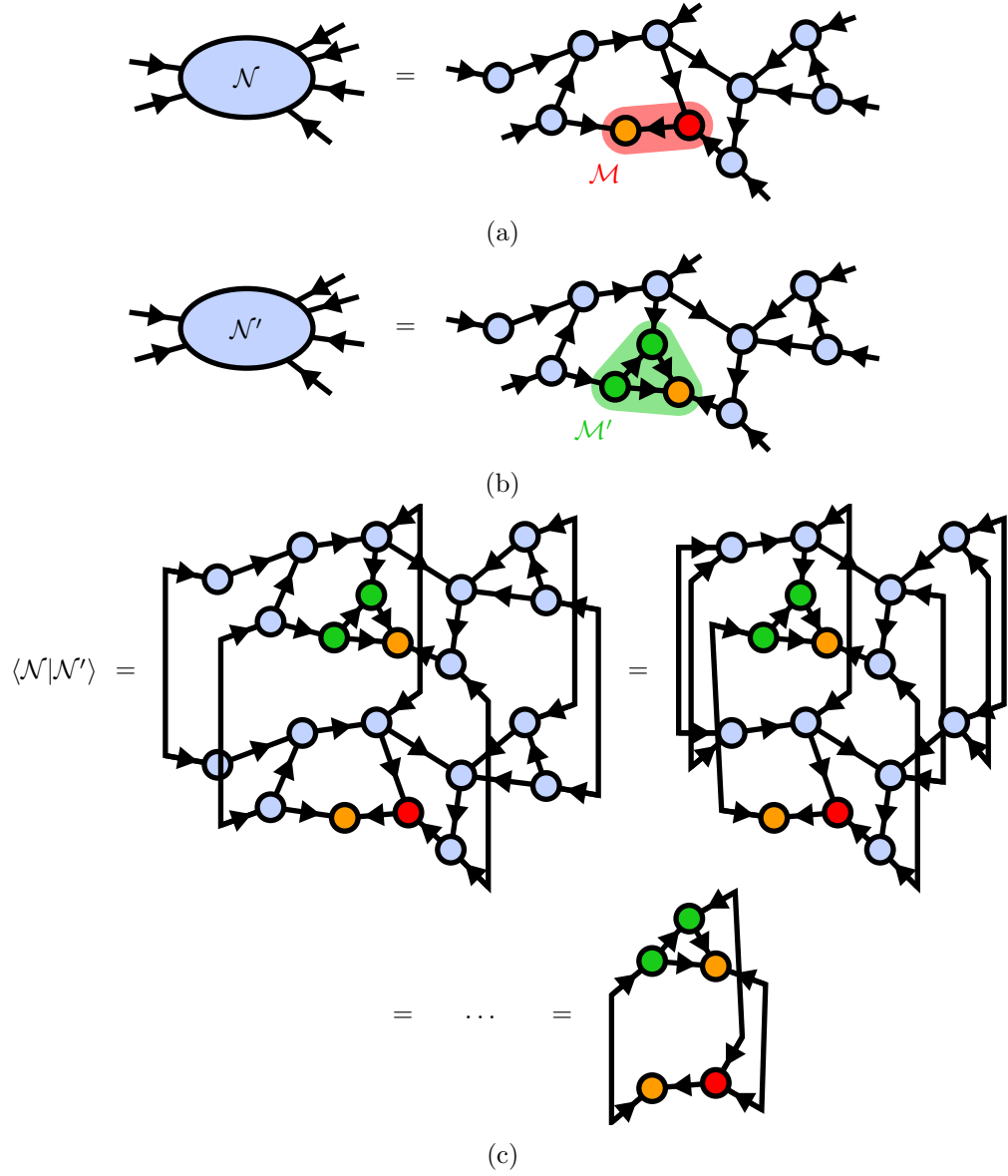


Figure 2.5: (a) An isometric tensor network \mathcal{N} with the orthogonality center depicted in orange. The sub-network \mathcal{M} is made up of all tensors in the red region. (b) The isometric tensor network \mathcal{N}' with an updated sub-network \mathcal{M}' . (c) The computation of the trace $\text{Tr}(\mathcal{N}\mathcal{N}')$ reduced to a contraction of the subregions $\text{Tr}(\mathcal{M}\mathcal{M}')$ because of the isometry condition.

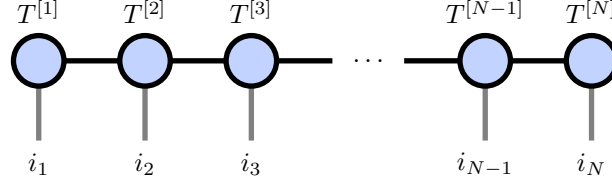


Figure 2.6: Diagrammatic representation of the Matrix Product State 2.11.

where N is the number of subsystems (e.g. lattice sites or particles), and $\{|i_1\rangle \otimes |i_2\rangle \otimes \cdots \otimes |i_N\rangle\}$, $i_j = 0, \dots, d_j$ is a set of basis vectors of the full many-body Hilbert space

$$\mathcal{H} = \bigotimes_{j=1}^N \mathcal{H}_j,$$

with $\dim(\mathcal{H}_j) = d_j$ the dimension of the local Hilbert space of subsystem j . To simplify the notation, we will assume that the dimension of all local subsystems is the same, $d_j = d$. The d^N complex numbers $\Psi_{i_1 i_2 \dots i_N}$ fully describe the quantum many-body state, and one can think of $\Psi \in \mathbb{C}^{d \times \cdots \times d}$ as a tensor of rank N . However, due to the size of the tensor scaling exponentially with system size, only very small system sizes are accessible computationally. One proceeds by writing Ψ as a tensor network of smaller tensors. A *Matrix Product State* (MPS) is constructed by introducing N rank-3 tensors $A^{[n]} \in \mathbb{C}^{d \times \chi_{n-1} \times \chi_n}$ and contracting them in a chain as

$$\Psi_{i_1 i_2 \dots i_N} := \sum_{\alpha_1=1}^{\chi_1} \sum_{\alpha_2=1}^{\chi_2} \cdots \sum_{\alpha_{N-1}=1}^{\chi_{N-1}} A_{1,\alpha_1}^{[1],i_1} A_{\alpha_1,\alpha_2}^{[1],i_2} \cdots A_{\alpha_{N-1},1}^{[N],i_N}, \quad (2.11)$$

where we have written the physical indices i_n as superscripts, such that the sums are performed only over subscripts. Note that in this notation the bond dimensions at the two ends of the chain is $\chi_0 = \chi_N = 1$, and we can interpret the tensors $A^{[1]}$ and $A^{[N]}$ as tensors of rank-2. A tensor diagram of the MPS (2.11) is given in figure 2.6. An important property of MPS is the existence of a *canonical form* as an isometric tensor network, where a single tensor $A^{[n]}$ is selected as the orthogonality center. One can bring an arbitrary MPS into this canonical form through successive QR-decompositions or SVDs, starting at the outer ends of the chain and isometrizing one tensor at a time, until the orthogonality center is reached [4]. In figure 2.7(a) an MPS in canonical with the orthogonality center at subsystem n is visualized in diagrammatic notation. The canonical form greatly simplifies many operations on MPS and allows for the formulation of efficient algorithms, where many contractions reduce to identity due to the isometry condition (2.5), see also figure 2.7(b). For example, the expectation value $\langle \Psi | \hat{O} | \Psi \rangle$ of a one-site operator

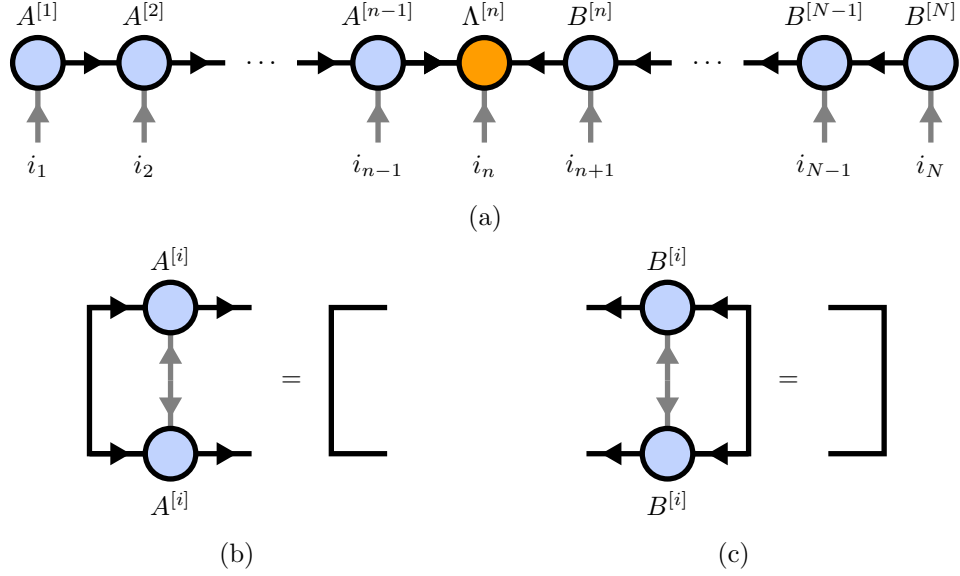


Figure 2.7: (a) Diagrammatic representation of an MPS in canonical form. (b) The isometry condition can be used to simplify contractions.

$\hat{O} \in \mathbb{C}^{d \times d}$ acting on site n can for a general MPS be computed as

$$\begin{aligned}
 \langle \Psi | \hat{O} | \Psi \rangle &= \sum_{i_1, \dots, i_N, j_n=1}^d \Psi_{i_1, i_2, \dots, i_N} \Psi_{i_1, \dots, i_{n-1}, j_n, i_{n+1}, \dots, i_N}^* \langle j_n | \hat{O} | i_n \rangle \\
 &= \sum_{i_1, \dots, i_N, j_n=1}^d \left(A^{[1], i_1} \dots A^{[N], i_N} \right) \\
 &\quad \cdot \left(A^{[1], i_1^*} \dots A^{[N], j_n^*} \dots A^{[N], i_N^*} \right) \cdot \hat{O}_{i_n, j_n},
 \end{aligned} \tag{2.12}$$

where the $A^{[n], i_n}$ are interpreted as matrices for $1 < n < N$ and as row/column vectors for $n = 1, N$ such that the product

$$\left(A^{[1], i_1} \dots A^{[N], i_N} \right)$$

gives a scalar. The contraction (2.12) is visualized as a tensor diagram in figure 2.8. Here, the advantage of the diagrammatic notation becomes apparent: It is much easier to understand how tensors are contracted when expressing the contraction in terms of tensor network diagrams. The computational cost of computing the expectation value like this scales linear with the system size $\mathcal{O}(N\chi^3d)$, where χ is the maximum virtual bond dimension $\chi = \max\{\chi_1, \dots, \chi_N\}$. If the MPS is however

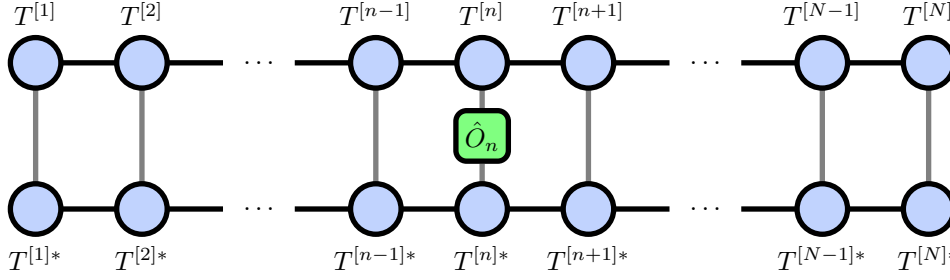


Figure 2.8: The computation of the expectation value of a local operator can be computed by contracting the MPS with its conjugate transpose, with the operator "sandwiched" between.

given in canonical form with the orthogonality center at site n , the computation reduces to a contraction of only three tensors as can be seen in figure 2.9, and the computational cost $\mathcal{O}(\chi^3 d)$ becomes independent of system size.

Until now, the MPS representation of $|\Psi\rangle$ is still exact. One can approximate a MPS by restricting the virtual bond dimension to a maximal bond dimension $\chi_n < \chi_{\max}$. In this case, the number of parameters that need to be stored to describe the state is reduced from $\mathcal{O}(d^N)$ to $\mathcal{O}(N\chi_{\max}^2 d)$. To arrive at this approximation, two neighbouring tensors can be contracted and split via a truncated SVD, keeping only the χ_{\max} largest singular values. If the orthogonality center of the MPS is at one of the two tensors, this approximation is globally optimal as explained in section 2.3. Additionally, this SVD at the orthogonality center is related to the Schimdt decomposition of a bipartite system

$$|\Psi\rangle = \sum_{\alpha=1}^{\chi_n} \lambda_{\alpha} \left| \Psi_{\alpha}^{[L]} \right\rangle \otimes \left| \Psi_{\alpha}^{[R]} \right\rangle,$$

where the chain is split into a left and right subsystem with orthogonal basis vectors $\left| \Psi_{\alpha}^{[L]} \right\rangle$ and $\left| \Psi_{\alpha}^{[R]} \right\rangle$ as visualized in figure ???. In this case, the Schmidt values $\lambda_{\alpha} \geq 0$ coincide with the singular values! One can further use this to compute the Von-Neumann entanglement entropy

$$S = - \sum_{\alpha=1}^{\chi_n} \lambda_{\alpha}^2 \log(\lambda_{\alpha}^2),$$

quantifying the amount of entanglement between the left and right subsystems. If the state is normalized, it additionally holds

$$\sum_{\alpha=1}^{\chi_n} \lambda_{\alpha}^2 = 1.$$

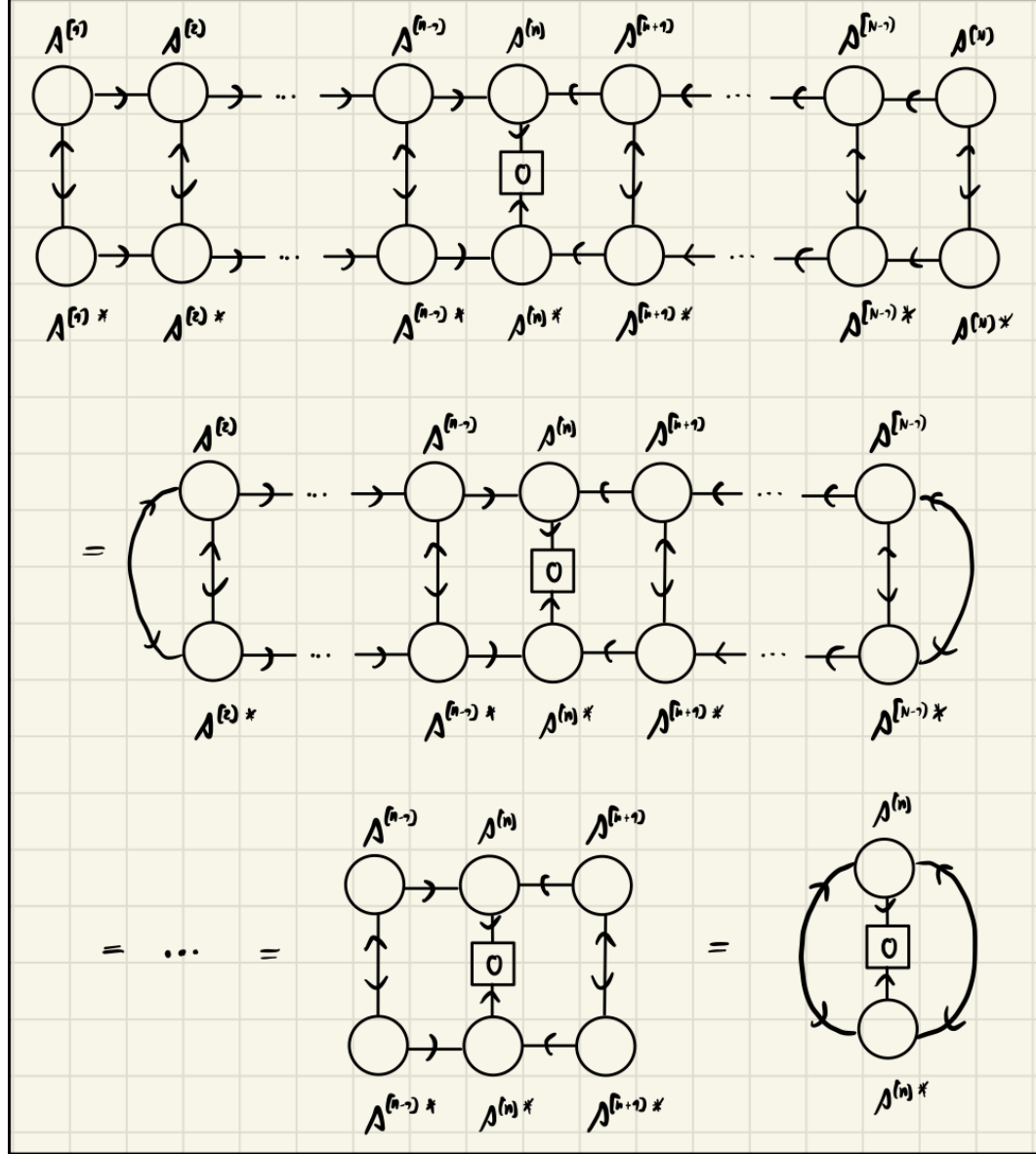


Figure 2.9: If the MPS is in canonical form, the computation of the expectation value of a local operator can be simplified to a contraction of three tensors using the isometry condition.

Thus, how well an MPS of a given bond dimension χ_{\max} is able to represent a given quantum state is highly dependent on the Schmidt spectrum $\{\lambda_\alpha\}$ at the different bipartitions of the chain. If the Schmidt values decrease exponentially, only an exponentially small part of the entanglement structure is truncated and the truncated MPS is a good approximation for the original state. It can be shown [7, 8] that for ground states of local, gapped, one dimensional Hamiltonians there holds an *area law*: The entanglement entropy at arbitrary bipartitions of the chain is bounded by a constant

$$S \leq S_{\max},$$

where S_{\max} is independent of the system size. This is in contrast to the fact that the entanglement of states drawn randomly from the many-body Hilbert space on average exhibits *volume law* scaling


$$\mathbb{E}[S] > \min(N_L, N_R) \log(d),$$

where N_L and N_R are the number of subsystems in the left and right bipartition. Hence, ground states of gapped Hamiltonians are very nongeneric. Note that the constant S_{\max} scales with the correlation length of the system, which diverges when approaching critical points.

It is immediately clear that truncated MPS by construction exhibit area law entanglement scaling, if the local subsystems that are represented by each tensor correspond to physical systems on a 1D chain. The maximal entanglement entropy for a bipartition can be reached when all Schmidt values are equal, $\lambda_\alpha = 1/\sqrt{\chi_n}$, and thus

$$S \leq \log(\chi_{\max})$$

for arbitrary bipartitions of the chain. One can conclude that MPS are good approximations for ground states of gapped 1D Hamiltonians away from criticality. For completeness we note that the truncation of all bonds of an MPS is a highly non-linear optimization problem and the naive algorithm of truncating each bond with an SVD does in general not lead to a minimal error. A variational compression procedure can often be used to obtain a lower error at the same maximum bond

 dimension χ_{\max} [4].

2.5 Isometric Tensor Product States in 2D

The natural generalization of MPS to higher dimensional lattices is given by *Projected Entangled Pair States* (PEPS). A PEPS is constructed similar to a MPS by representing the local subsystem on each lattice site i with the index σ_i of a

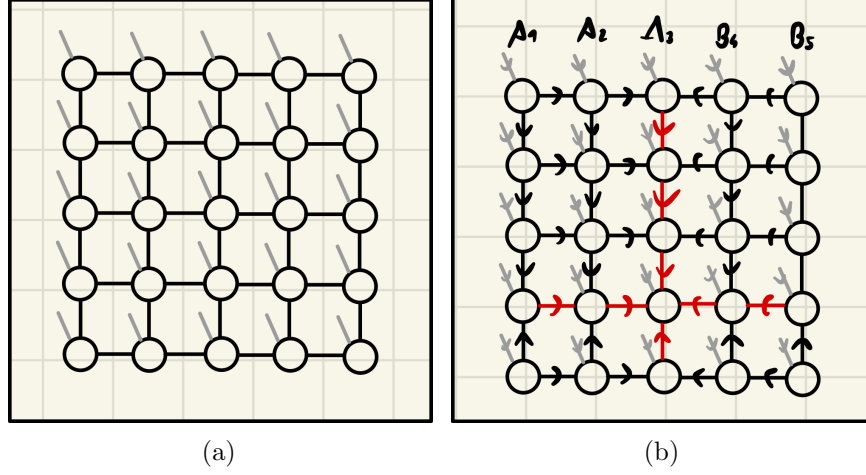


Figure 2.10: Tensor Networks representing two dimensional states on a square lattice. (a) A Projected Entangled Pair State (PEPS). (b) An isometric Tensor Product State (isoTPS).

tensor $T_i^{\sigma_i}$ and connecting nearest-neighbour tensors with virtual bonds. The quantum state can then be written as

$$|\Psi\rangle = \sum_{\sigma_1, \sigma_2, \dots, \sigma_N} \mathcal{C}(T_1^{\sigma_1}, T_2^{\sigma_2}, \dots, T_N^{\sigma_N}) |\sigma_1, \sigma_2, \dots, \sigma_N\rangle,$$

where $\mathcal{C}(\dots)$ denotes the contraction of the full network along all virtual bonds. As an example, we draw a PEPS on a square lattice in figure 2.10a.

PEPS are able to efficiently represent area-law states in two and higher dimensions [5]. Remarkably, PEPS can even handle correlations decaying polynomially with separation distance [9], whereas MPS can only handle exponentially decaying correlations. Polynomially decaying correlations are characteristic for critical points. Unfortunately, it is not generally possible to bring a PEPS into an exact canonical form due to the presence of closed loops. Thus, already the computation of local expectation values scales exponentially with system size and can in practice be only done approximately, e.g. using the boundary MPS method [5] or corner transfer matrices [10]. Moreover, algorithms for ground state search and time evolution have computational costs scaling with high powers of the bond dimension. For example the cost of a full update TEBD or DMRG iteration is dominated by the contraction of an effective environment, scaling as $\mathcal{O}(D^{10})$ [11].

Recently, the new class of *isometric Tensor Product States* (isoTPS) has been introduced [1, 12, 13], generalizing the canonical form of MPS to higher dimensions by enforcing isometry constraints. This allows for efficient computation of local

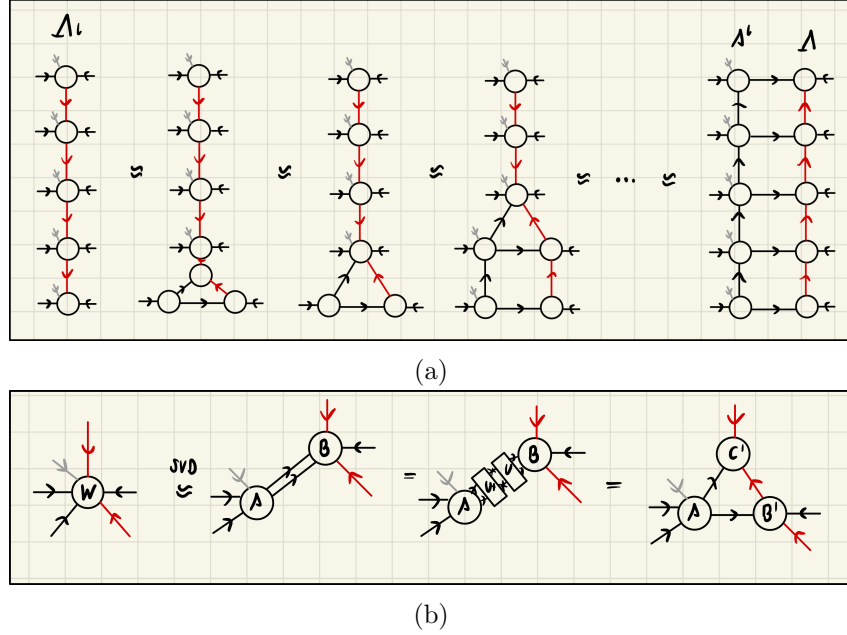


Figure 2.12: (a) The Moses Move (MM) splits the column Λ_l into A_l and Λ via a single unzipping sweep of tripartite decompositions. (b) Tripartite decomposition of the tensor W as explained in the text.

orthogonality hypersurface B_l , with $l = 1, 2, \dots, L$ and L the linear system size. Moving the orthogonality hypersurface Λ_l one column to the right can be expressed as solving the problem

$$\Lambda_l B_{l+1} = A_l \Lambda_{l+1}, \quad (2.13)$$

where the notation $\Lambda_l B_{l+1}$ means the contraction of columns Λ_l and B_{l+1} along their connecting bonds. Instead of (2.13), one can solve the simpler auxillary problem

$$\Lambda_l = A^l \Lambda, \quad (2.14)$$

where Λ is a column of tensors with no physical indices, as shown in figure 2.11b. This column can then be absorbed into B_{l+1} via the standard algorithm of applying an MPO to an MPS and subsequent MPS compression [4]. One can variationally solve problem (2.14) by minimizing the distance $|\Lambda_l - A_l \Lambda|$, sweeping back and forth through the tensors while respecting the isometry condition. It is however found in [1] that a single unzipping sweep, called the *Moses Move* (MM), provides a solution very close to the variational one whilst being far quicker. The MM can also be used as a good initialization for the variational algorithm. We sketch the MM in figure 2.12a. We start from the bottom of the orthogonality hypersurface column

and split the tensors one after the other using a tripartite decomposition. A single tripartite decomposition of a tensor W is shown in figure 2.12b. First, W is split into two tensors A and B via a truncated SVD $W = U(SV) = AB$ with A an isometry. The bond connecting A and B is reshaped into two bonds. Next, it is important to note that the full contraction is invariant under the insertion of a unitary and its conjugate transpose, $AB = (AU^\dagger)(UB)$, with (AU^\dagger) still satisfying the isometry condition. This degree of freedom can be used to *disentangle* the tensor B along the direction of the red bonds. Accordingly, we choose U such that the truncation error or some entanglement measure is minimized for splits along the direction of the red bonds. Choosing a good disentangling unitary is crucial for a successful tripartite decomposition and will be discussed further in section ??.

Assume for now that a good disentangling unitary has been found. After contracting (AU^\dagger) and (UB) , a truncated SVD is used to split (UB) into tensors B' and C' as shown in figure 2.12b, completing the tripartite decomposition.

Because the orthogonality center can be moved easily along the orthogonality hypersurface, one can think of the orthogonality hypersurface along a column or row as a 1D MPS with an enlarged physical bond dimension grouping together the physical and the two ancilla legs protruding from the orthogonality hypersurface tensors. Standard MPS algorithms can then be generalized to isoTPS by performing one iteration of the algorithm on the orthogonality hypersurface MPS, before moving the hypersurface via MM or variational optimization and repeating the procedure. As an example, we will discuss TEBD^2 , the generalization of TEBD to an isoTPS on a 2D square lattice.

isoTPS are a new class of states that enable the implementation of faster algorithms for e.g. ground state search and time evolution, compared to PEPS. The expressional power of isoTPS has been studied in [14], where it was found that isoTPS with finite bond dimension can exactly represent ground state wavefunctions of string-net liquid models, showing that long-range entanglement does not form an obstruction for isoTPS representations and suggesting that the ground states of gapped Hamiltonians with gappable edges can be efficiently represented as an isoTPS. There have also been works discussing the computational complexity of isoTNS [15] and relating isoTNS to quantum circuits [16, 17]. In [18], topological phase transitions were studied with isoTPS, showing that isoTPS can represent some critical states with power-law correlations. A DMRG²-algorithm was implemented on isoTPS in [2] and used to compute dynamical structure factors of ground states using real time evolution. IsoTPS were also extended to fermionic systems [19], to two dimensional strips of infinite length [20], and to three dimensional cubic lattices [21]. They have also been used to compute properties of two dimensional thermal states [22].

Chapter 3

diagonal isometric Tensor Product States (disoDTPS)

In the following, we will introduce a new class of isometric tensor tensor states which we call *diagonal isometric tensor product states* (disoTPS). This class of tensor product states is in many ways similar to the isometric tensor product states discussed in section 2.5, with some important differences.

3.1 Network Structure

The structure of a disoTPS on a square lattice is shown in figure 3.1. It can be constructed in three steps. First, a square PEPS is rotated by 45° . Next, the orthogonality hypersurface is constructed as a column of auxillary tensors. The auxillary tensors are connected in a line similar to an MPS and placed between between two columns of PEPS tensors. Note that, in contrast to the standard isoTPS the tensors of the orthogonality hypersurface do not carry any physical degrees of freedom and are only connected via virtual bonds to the neighboring tensors. Lastly, the isometry condition is enforced such that all arrows point towards the orthogonality hypersurface. Tensors left of the orthogonality surface are thus brought into a left-isometric form and tensors right of the orthogonality surface are brought into a right-isometric form, as shown in figure 3.1. The auxillary tensors making up the orthogonality hypersurface are isometrized such that all arrows point towards a single auxillary tensor, the orthogonality center.

In the following, we will denote the auxillary tensors by W_i , and the tensors carrying physical degrees of freedom with T_i . The bonds connecting two T -tensors or a T -tensor and a W -tensor are truncated to a maximal bond dimension of D , while the maximal bond dimension between two W -tensors is denoted as χ . In practice it is found that setting $\chi = f \cdot D$ with an integer $f \geq 1$ produces good results.

Similar to the standard isoTPS, the orthogonality center can easily and exactly be moved along the orthogonality hypersurface using QR-decompositions. Moving the orthogonality hypersurface to the left or to the right is a harder problem and will be discussed in section 3.2.

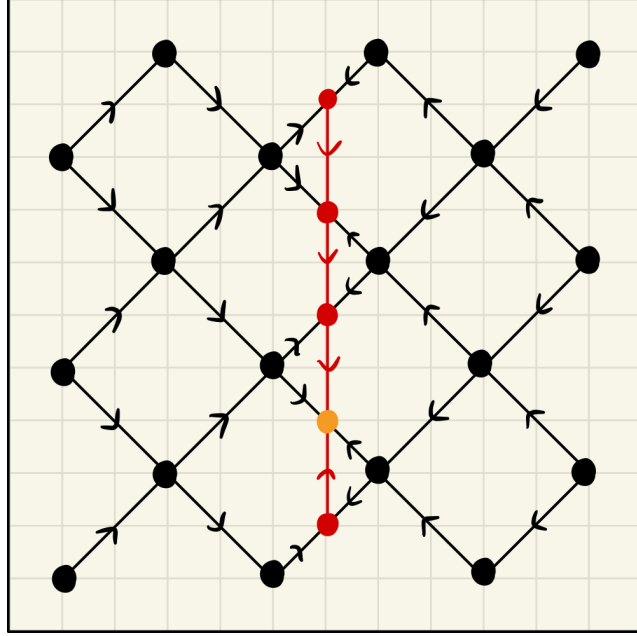


Figure 3.1: A diagonal isometric tensor network on a square lattice is constructed from site tensors T_i (drawn in black) and an orthogonality hypersurface of auxiliary tensors W_i (drawn in red). The orthogonality hypersurface is rotated by 45° with respect to the lattice.

As in MPS and standard isoTPS, disoTPS allow for the fast computation of expectation values of local operators. The expectation value $\langle \Psi | \hat{O}_i | \Psi \rangle$ of a one-site operator \hat{O}_i acting on site i can be computed as follows: First, the orthogonality center is moved next to site i . We next define the *one-site wavefunction* as the sub-network containing the site tensor T_i and the two connected W -tensors. Note that the one-site wavefunction is connected to its environment only by bonds with incoming arrows. Next the wavefunction is contracted with its complex conjugate, sandwiching the operator \hat{O}_i between the two. Due to the isometry condition, this reduces to a contraction of only the one-site wavefunction, its complex conjugate, and the operator \hat{O}_i , as shown in figure 3.2. This contraction has a computational cost scaling as $\mathcal{O}(\chi^3 D^3 + D^6 d^2)$ and gives as result the desired expectation value. The expectation value $\langle \Psi | \hat{O}_{ij} | \Psi \rangle$ of a two-site operator \hat{O}_{ij} acting on two neighbouring sites i and j , also called *bond operator*, can be computed similarly. First, the orthogonality center is moved such that it sits in the middle of the bond connecting sites i and j . The *two-site wavefunction* is then defined as the subnetwork containing the two site tensors T_i and T_j and three W -tensors as shown in figure 3.3, such that again all legs connecting the subnetwork to its environment

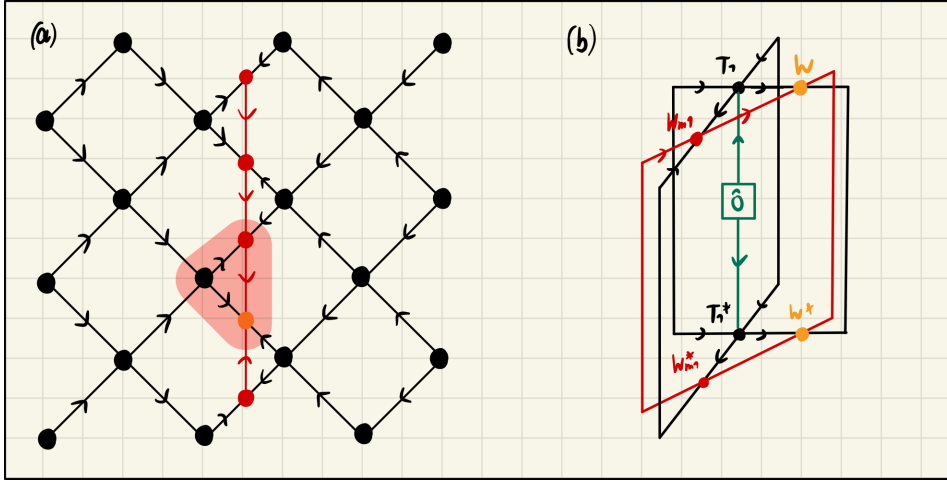


Figure 3.2: (a) The one-site wavefunction around a site i is the sub network containing the site tensor T_i and the two connected auxillary tensors. (b) Computation of a single site expectation value reduces to the shown contraction over a one-site wavefunction, its complex conjugate, and the one-site operator \hat{O}_i .

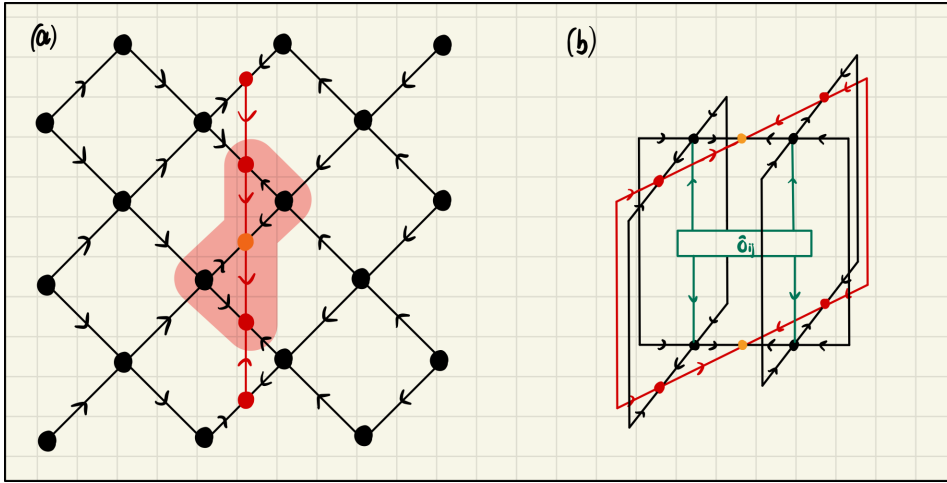


Figure 3.3: (a) The two-site wavefunction around neighboring sites i and j is the sub network containing the site tensors T_i and T_j and the three connected auxillary tensors. (b) Computation of a two-site expectation value reduces to the shown contraction over a two-site wavefunction, its complex conjugate, and the two-site operator \hat{O}_{ij} .

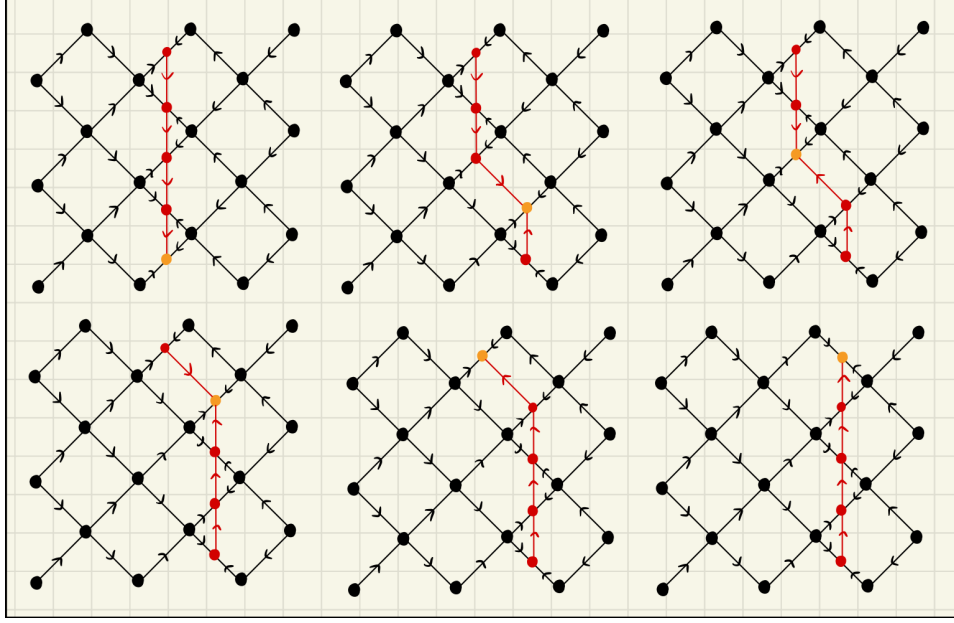


Figure 3.4: Two YB-moves are used to shift the orthogonality hypersurface one column to the right. In the last step, the orthogonality center can be moved across the T -tensor by contracting the two tensors and performing a QR-decomposition.

are only decorated with arrows pointing towards the two-site wavefunction. The computation of the expectation value then reduces to the contraction of only the two-site wavefunction with its complex conjugate and the bond operator \hat{O}_{ij} . The computational cost of this contraction scales as $\mathcal{O}(\chi^3 D^3 d^2)$.

3.2 Yang-Baxter Move

Most algorithms implemented on disoTPS require an efficient procedure for moving the orthogonality surface, where the error introduced by this procedure should be as small as possible. For isoTPS, the current best procedure is given by the Moses Move, followed by an optional variational optimization.

In analogy to the MM we look for a procedure to iteratively shift the orthogonality surface through one column of T -tensors as shown in figure 3.4. A single iteration of this process is shown in figure 3.5. The two tensors W_1 and W_2 , which are part of the orthogonality hypersurface, are "pulled through" the site tensor T , resulting in the updated tensors T' , W'_1 and W'_2 . To keep the isometric structure of the network, T' and W'_1 must be isometries, while W'_2 must be a tensor of norm one (the new

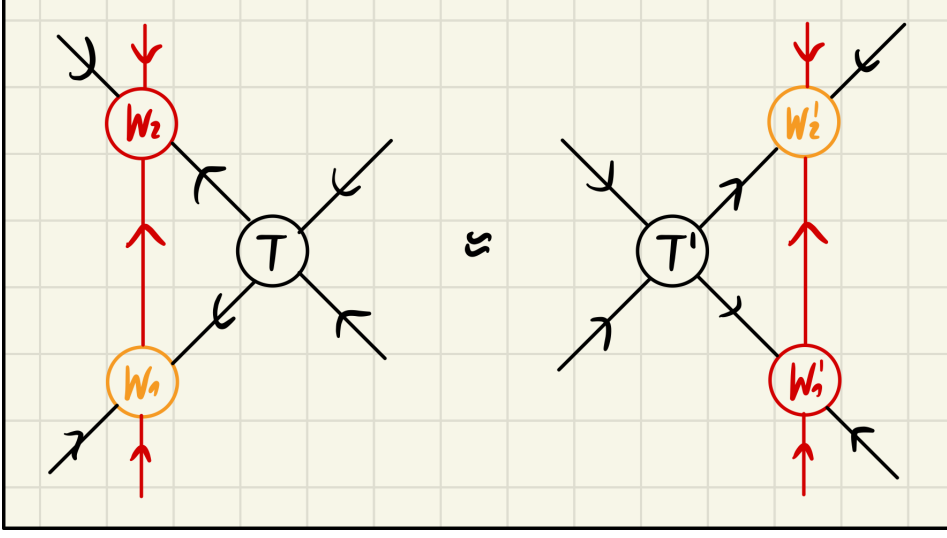


Figure 3.5: The Yang-Baxter (YB) move is the procedure of "pulling" two auxillary tensors W_1 and W_2 through a site tensor T .

orthogonality center). Due to the visual similarity to the Yang-Baxter equation we call this procedure the *Yang-Baxter* (YB) move.

We denote the state represented by the disoTPS before the YB move by $|\Psi\rangle = |\Psi(W_1, W_2, T)\rangle$ and the state after the YB move by $|\Psi'\rangle = |\Psi'(W'_1, W'_2, T')\rangle$. One can think of the YB move as a constrained optimization problem

$$(T', W'_1, W'_2) = \min_{T', W'_1, W'_2} \| |\Psi\rangle - |\Psi'\rangle \|, \quad (3.1)$$

$$T'^{\dagger}T' = \mathbb{1}, \quad W_1'^{\dagger}W'_1 = \mathbb{1}, \quad \|W'_2\| = 1. \quad (3.2)$$

In the following, we present two explicit algorithms for performing the YB move. The first algorithm is an iterative optimization using local updates respecting the constraints. The second algorithm is a tripartite decomposition with disentangling similar to the tripartite decomposition used in the MM. In section ?? we will compare the two algorithms.

3.2.1 Iterative optimization with local updates

We can rewrite the error of the YB move as

$$\begin{aligned} \| |\Psi\rangle - |\Psi'\rangle \|_F &= \sqrt{\langle \Psi | \Psi \rangle + \langle \Psi' | \Psi' \rangle - 2 \operatorname{Re} \langle \Psi | \Psi' \rangle} \\ &= \sqrt{2 - 2 \operatorname{Re} \langle \Psi | \Psi' \rangle}, \end{aligned}$$

where in the second step we used the fact that the wave function is normalized to one, $\langle \Psi | \Psi \rangle = \langle \Psi' | \Psi' \rangle = 1$. It follows that the optimization problem of minimizing the error becomes the problem of maximizing the overlap

$$(T', W'_1, W'_2) = \underset{T', W'_1, W'_2}{\operatorname{argmax}} \operatorname{Re} \langle \Psi | \Psi' \rangle$$

under the constraints (3.2). Because the only tensors that are changed by the YB move are W_1 , W_2 and T and the three tensors make up a subregion of the full network with only incoming arrows, we can use the isometry condition and the computation of the overlap reduces to a contraction of only six tensors as shown in figure 3.6a. We proceed by keeping all tensors fixed except one of the three tensors T' , W'_1 or W'_2 and optimizing the overlap. We can then iterate over the three tensors to converge to a solution.

We first show how the tensor W'_2 can be optimized. We treat all tensors except W'_2 as constant and contract them into an environment E as shown in figure 3.6b. One can then write the optimization problem as

$$W'_2 = \underset{\|W'_1\|=1}{\operatorname{argmax}} \operatorname{Re} \langle \Psi | \Psi' \rangle = \underset{\|W'_1\|=1}{\operatorname{argmax}} \operatorname{Re} \langle W'_2, E \rangle_{\text{F}}, \quad (3.3)$$

with the Frobenius inner product $\langle \cdot, \cdot \rangle_{\text{F}}$ (2.6). The Frobenius inner product satisfies the Cauchy-Schwarz inequality and we obtain

$$|\operatorname{Re} \langle W'_2, E \rangle_{\text{F}}| \leq \|W'_2\| \|E\| = \|E\|.$$

If we set $W = E/\|E\|$ we obtain

$$\operatorname{Re} \langle W'_2, E \rangle_{\text{F}} = \frac{\operatorname{Re} \langle E', E \rangle_{\text{F}}}{\|E\|} = \|E\|$$

and the maximum is reached. Thus, the closed form solution to (3.3) is $W'_2 = E/\|E\|$.

Next, we optimize the tensor W'_1 . Again, we keep all other tensors fixed and contract them into the environment E as shown in figure 3.6c. We now reshape E into a matrix, grouping together all legs that connect to legs of W'_1 decorated with incoming/outgoing arrows respectively (see figure 3.6c). For the bond dimensions specified in figure 3.6a, E is a complex $\chi D^2 \times \chi$ matrix. The optimization problem can then be written as

$$W'_1 = \underset{W_1'^{\dagger} W_1' = \mathbb{1}}{\operatorname{argmax}} \operatorname{Re} \langle \Psi | \Psi' \rangle = \underset{W_1'^{\dagger} W_1' = \mathbb{1}}{\operatorname{argmax}} \operatorname{Re} \langle W'_1, E \rangle_{\text{F}} = \underset{W_1'^{\dagger} W_1' = \mathbb{1}}{\operatorname{argmax}} \operatorname{Re} \operatorname{Tr} (W_1'^{\dagger} E),$$

where W'_1 has the same dimensions as E . This is known as the *orthogonal procrustes problem* and permits a closed-form solution. Making the SVD of E yields

$E = USV^\dagger$. Note that, because of the shape of E , V is a $\chi \times \chi$ unitary. Inserting the SVD into the trace yields


$$\begin{aligned} \text{Re Tr} \left(W_1'^\dagger E \right) &= \text{Re Tr} \left(E W_1'^\dagger \right) = \text{Re Tr} \left(U S V^\dagger W_1'^\dagger \right) \\ &= \text{Re Tr} \left[\left(U \sqrt{S} \right) \left(\sqrt{S} V^\dagger W_1'^\dagger \right) \right] = \text{Re} \left\langle \sqrt{S} U^\dagger, \sqrt{S} V^\dagger T'^\dagger \right\rangle_{\text{F}}. \end{aligned}$$

We again use the Cauchy-Schwarz inequality to obtain an upper bound

$$\begin{aligned} \left| \text{Re Tr} \left(W_1'^\dagger E \right) \right| &= \left| \text{Re} \left\langle \sqrt{S} U^\dagger, \sqrt{S} V^\dagger T'^\dagger \right\rangle_{\text{F}} \right| \leq \left\| \sqrt{S} U^\dagger \right\|_{\text{F}} \left\| \sqrt{S} V^\dagger T'^\dagger \right\|_{\text{F}} \\ &= \sqrt{\text{Tr} (U S U^\dagger) \text{Tr} (T' V S V^\dagger T'^\dagger)} = \text{Tr} (S), \end{aligned}$$

where in the last step we used $U^\dagger U = \mathbb{1}$, $V^\dagger V = \mathbb{1}$, $W_1'^\dagger W_1' = \mathbb{1}$ and the cyclic property of the trace. The upper bound can be reached by setting $W_1' = UV^\dagger$:

$$\text{Re Tr} \left(W_1'^\dagger E \right) = \text{Re Tr} \left(V U^\dagger U S V^\dagger \right) = \text{Tr} (S).$$

Lastly we show how the tensor T' can be optimized. Similar to the optimization of W_1' , we obtain an orthogonal Procrustes problem after contracting the environment E and performing an SVD $E = USV^\dagger$ as shown in figure 3.6d. Again, the closed form solution is given by $T' = UV^\dagger$. To summarize, the complete procedure is given in algorithm 1. In practice, one can compute the remaining error after each iteration and terminate the while loop if the decrease in error is smaller than a given threshold or if a given maximum number of iterations is reached. 

Algorithm 1 iterative YB optimization with local updates

Input: tensors $T, W_1, W_2, T', W_1', W_2'$ as in figure 3.6a

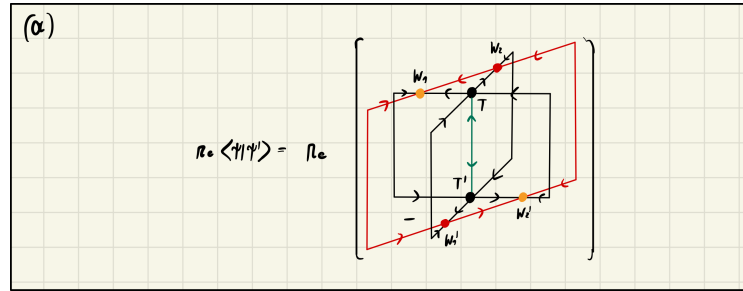
Output: Optimized tensors T', W_1', W_2' minimizing the truncation error (3.1)

```

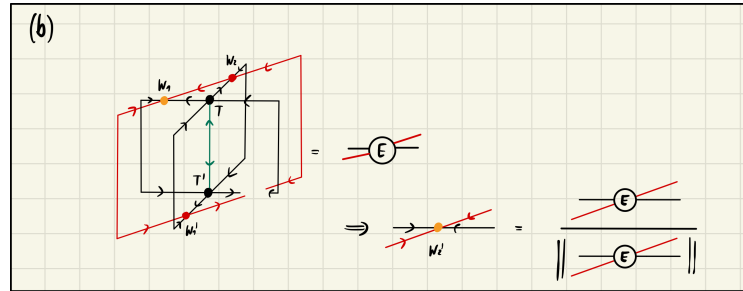
while not converged do
   $E \leftarrow \text{contract} (T, W_1, W_2, W_1', W_2')$ 
   $U, S, V^\dagger \leftarrow \text{SVD} (E)$ 
   $T' \leftarrow UV^\dagger$ 
   $E \leftarrow \text{contract} (T, W_1, W_2, T', W_2')$ 
   $U, S, V^\dagger \leftarrow \text{SVD} (E)$ 
   $W_1' \leftarrow UV^\dagger$ 
   $E \leftarrow \text{contract} (T, W_1, W_2, T', W_1')$ 
   $W_2' \leftarrow E / \|E\|$ 
end while

```

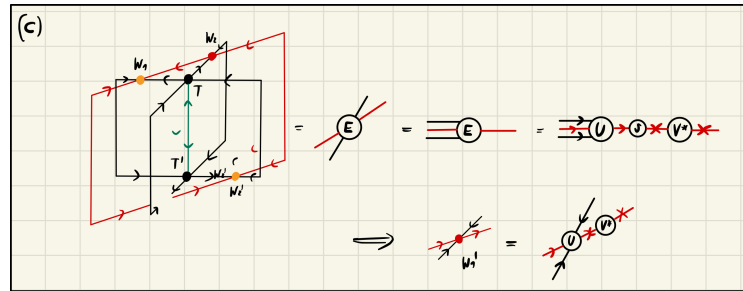
3.3 Time Evolving Block Decimation (TEBD)



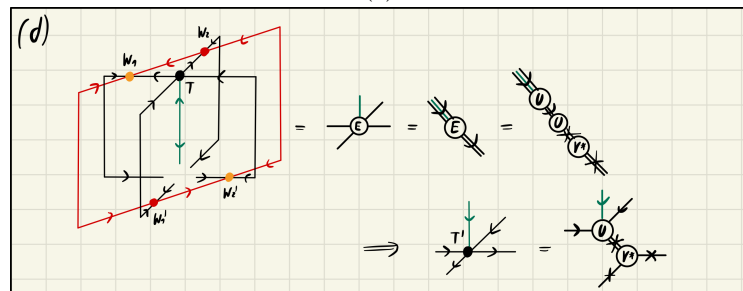
(a)




(b)



(c)



(d)

Figure 3.6: 

Chapter 4

Toric Code: An exactly representable Model

Chapter 5

Transverse Field Ising Model: Ground State Search and Time Evolution

Appendix A

Riemannian Optimization of Isometries

In this appendix we provide a brief introduction to the problem of optimizing a cost function on the constrained set of isometric matrices. This problem can be solved by performing Riemannian Optimization on the matrix manifold of isometric matrices, which is called the Stiefel manifold. For a more in-depth introduction to the topic we recommend the excellent book [23]. A discussion of Riemannian optimization of complex matrix manifolds in the context of quantum physics and isometric tensor networks can be found at [24, 25]. An implementation of Riemannian Optimization on the real Stiefel manifold and other matrix manifolds in python is given in [26]. Some parts of this implementation were also used in our implementation.

A.1 The complex Stiefel manifold

We define the *complex Stiefel manifold* $\text{St}(n, p)$ with $n \geq p$ as the set of all isometric $n \times p$ matrices:

$$\text{St}(n, p) := \left\{ X \in \mathbb{C}^{n \times p} : X^\dagger X = \mathbb{1} \right\}.$$

In particular, for $n = p$, the complex Stiefel manifold reduces to the set of unitary matrices $U(n)$. One can show, similar to [23], that the complex Stiefel manifold is naturally an embedded submanifold of the Euclidian vector space $\mathbb{C}^{n \times p} \cong \mathbb{R}^{2np}$ of general complex $n \times p$ matrices.

Tangent vectors on manifolds generalize the notion of directional derivatives. A mathematical definition of tangent vectors and tangent spaces of manifolds is given in [23]. The set of all tangent vectors to a point $X \in \text{St}(n, p)$ is called the *tangent space* $T_X \text{St}(n, p)$, which is given by [23, 25]

$$T_X \text{St}(n, p) = \left\{ Z \in \mathbb{C}^{n \times p} : X^\dagger Z + Z^\dagger X = 0 \right\}.$$

An arbitrary element $\xi \in \mathbb{C}^{n \times p}$ from the embedding space $\mathbb{C}^{n \times p}$ can be projected to the tangent space $T_X \text{St}(n, p)$ by [23, 25]

$$P_X \xi = \xi - \frac{1}{2} X \left(X^\dagger \xi + \xi^\dagger X \right). \quad (\text{A.1})$$

Additionally, we will also need to define a notion of length that we can apply to tangent vectors. This can be done in the form of an *inner product* on tangent spaces, called the *Riemannian metric*. A natural metric for the tangent space $T_X \text{St}(n, p)$ of the Stiefel manifold is the Euclidean metric of the embedding space $\mathbb{C}^{n \times p}$, which is given by the real part of the Frobenius inner product:

$$g_W : T_X \text{St}(n, p) \times T_X \text{St}(n, p) \rightarrow \mathbb{R}, \quad g_X(\xi_1, \xi_2) = \text{Re Tr} \left(\xi_1^\dagger \xi_2 \right). \quad (\text{A.2})$$

Equipped with a Riemannian metric the Stiefel manifold becomes a Riemannian submanifold of $\mathbb{C}^{n \times p}$.

With these definition, we can now formulate the optimization problem as the problem of finding the isometry $W_{\text{opt}} \in \text{St}(n, p)$ that minimizes the cost function

$$f : \text{St}(n, p) \rightarrow \mathbb{R}, \quad X \mapsto f(X). \quad (\text{A.3})$$

A.2 Gradients, retractions, and vector transport

First order optimization algorithms like Gradient Descent and Conjugate Gradients use the gradient of the cost function to update the search direction at each iteration. In the case of the Stiefel manifold and the cost function (A.3), we first define the matrix of partial derivatives $D \in \mathbb{C}^{n \times p}$ of f at $X \in \text{St}(n, p)$ by

$$D_{ij} := \left. \frac{\partial f}{\partial \text{Re}(X_{ij})} \right|_X + i \left. \frac{\partial f}{\partial \text{Im}(X_{ij})} \right|_X. \quad (\text{A.4})$$

With this definition, the directional derivative $Df(X)[Z]$ at $X \in \text{St}(n, p)$ in direction $Z \in \mathbb{C}^{n \times p}$ is simply given by an inner product of D with the direction Z , using the Riemannian metric (A.2):

$$\begin{aligned} g_X(D, Z) &= \text{Re Tr} \left(D^\dagger Z \right) = \text{Re} \sum_{ij} D_{ij}^* Z_{ij} \\ &= \sum_{ij} \left(\left. \frac{\partial f}{\partial \text{Re}(X_{ij})} \right|_X \text{Re } Z_{ij} + \left. \frac{\partial f}{\partial \text{Im}(X_{ij})} \right|_X \text{Im } Z_{ij} \right) \\ &=: Df(X)[Z]. \end{aligned}$$

With this we can now define the gradient $\nabla f(X)$ of f at $X \in \text{St}(n, p)$ as the projection of the partial derivative matrix (A.4) to the tangent space [23, 25]:

$$\nabla f(X) := P_X D = D - \frac{1}{2} X \left(X^\dagger D + D^\dagger X \right),$$

where we used the projection (A.1).

A.3 Conjugate Gradients

A.4 Trust Region Method

Appendix B

Initialization of the Disentangling Unitary

Bibliography

- [1] Michael P. Zaletel and Frank Pollmann. ‘Isometric Tensor Network States in Two Dimensions’. In: *Phys. Rev. Lett.* 124 (3 Jan. 2020), p. 037201. DOI: 10.1103/PhysRevLett.124.037201. URL: <https://link.aps.org/doi/10.1103/PhysRevLett.124.037201>.
- [2] Sheng-Hsuan Lin, Michael P. Zaletel and Frank Pollmann. ‘Efficient simulation of dynamics in two-dimensional quantum spin systems with isometric tensor networks’. In: *Phys. Rev. B* 106 (24 Dec. 2022), p. 245102. DOI: 10.1103/PhysRevB.106.245102. URL: <https://link.aps.org/doi/10.1103/PhysRevB.106.245102>.
- [3] Carl Eckart and Gale Young. ‘The approximation of one matrix by another of lower rank’. In: *Psychometrika* 1.3 (1936), pp. 211–218.
- [4] Ulrich Schollwöck. ‘The density-matrix renormalization group in the age of matrix product states’. In: *Annals of physics* 326.1 (2011), pp. 96–192.
- [5] Román Orús. ‘A practical introduction to tensor networks: Matrix product states and projected entangled pair states’. In: *Annals of physics* 349 (2014), pp. 117–158.
- [6] Johannes Hauschild and Frank Pollmann. ‘Efficient numerical simulations with Tensor Networks: Tensor Network Python (TeNPy)’. In: *SciPost Phys. Lect. Notes* (2018), p. 5. DOI: 10.21468/SciPostPhysLectNotes.5. URL: <https://scipost.org/10.21468/SciPostPhysLectNotes.5>.
- [7] M B Hastings. ‘An area law for one-dimensional quantum systems’. In: *Journal of Statistical Mechanics: Theory and Experiment* 2007.08 (Aug. 2007), P08024. DOI: 10.1088/1742-5468/2007/08/P08024. URL: <https://dx.doi.org/10.1088/1742-5468/2007/08/P08024>.
- [8] J. Eisert, M. Cramer and M. B. Plenio. ‘Colloquium: Area laws for the entanglement entropy’. In: *Rev. Mod. Phys.* 82 (1 Feb. 2010), pp. 277–306. DOI: 10.1103/RevModPhys.82.277. URL: <https://link.aps.org/doi/10.1103/RevModPhys.82.277>.
- [9] F. Verstraete et al. ‘Criticality, the Area Law, and the Computational Power of Projected Entangled Pair States’. In: *Phys. Rev. Lett.* 96 (22 June 2006), p. 220601. DOI: 10.1103/PhysRevLett.96.220601. URL: <https://link.aps.org/doi/10.1103/PhysRevLett.96.220601>.

- [10] RJ Baxter and IG Enting. ‘Series expansions from corner transfer matrices: the square lattice ising model’. In: *Journal of Statistical Physics* 21 (1979), pp. 103–123.
- [11] Michael Lubasch, J Ignacio Cirac and Mari-Carmen Banuls. ‘Unifying projected entangled pair state contractions’. In: *New Journal of Physics* 16.3 (2014), p. 033014.
- [12] Reza Haghshenas, Matthew J. O’Rourke and Garnet Kin-Lic Chan. ‘Conversion of projected entangled pair states into a canonical form’. In: *Phys. Rev. B* 100 (5 Aug. 2019), p. 054404. DOI: 10.1103/PhysRevB.100.054404. URL: <https://link.aps.org/doi/10.1103/PhysRevB.100.054404>.
- [13] Katharine Hyatt and E. M. Stoudenmire. *DMRG Approach to Optimizing Two-Dimensional Tensor Networks*. 2020. arXiv: 1908.08833 [cond-mat.str-el]. URL: <https://arxiv.org/abs/1908.08833>.
- [14] Tomohiro Soejima et al. ‘Isometric tensor network representation of string-net liquids’. In: *Phys. Rev. B* 101 (8 Feb. 2020), p. 085117. DOI: 10.1103/PhysRevB.101.085117. URL: <https://link.aps.org/doi/10.1103/PhysRevB.101.085117>.
- [15] Daniel Malz and Rahul Trivedi. *Computational complexity of isometric tensor network states*. 2024. arXiv: 2402.07975 [quant-ph]. URL: <https://arxiv.org/abs/2402.07975>.
- [16] Zhi-Yuan Wei, Daniel Malz and J. Ignacio Cirac. ‘Sequential Generation of Projected Entangled-Pair States’. In: *Phys. Rev. Lett.* 128 (1 Jan. 2022), p. 010607. DOI: 10.1103/PhysRevLett.128.010607. URL: <https://link.aps.org/doi/10.1103/PhysRevLett.128.010607>.
- [17] Lucas Slattery and Bryan K. Clark. *Quantum Circuits For Two-Dimensional Isometric Tensor Networks*. 2021. arXiv: 2108.02792 [quant-ph]. URL: <https://arxiv.org/abs/2108.02792>.
- [18] Yu-Jie Liu, Kirill Shtengel and Frank Pollmann. *Topological quantum phase transitions in 2D isometric tensor networks*. 2024. arXiv: 2312.05079 [quant-ph]. URL: <https://arxiv.org/abs/2312.05079>.
- [19] Zhehao Dai et al. *Fermionic Isometric Tensor Network States in Two Dimensions*. 2024. arXiv: 2211.00043 [cond-mat.str-el]. URL: <https://arxiv.org/abs/2211.00043>.
- [20] Yantao Wu et al. ‘Two-dimensional isometric tensor networks on an infinite strip’. In: *Phys. Rev. B* 107 (24 June 2023), p. 245118. DOI: 10.1103/PhysRevB.107.245118. URL: <https://link.aps.org/doi/10.1103/PhysRevB.107.245118>.

- [21] Maurits S. J. Tepaske and David J. Luitz. ‘Three-dimensional isometric tensor networks’. In: *Phys. Rev. Res.* 3 (2 June 2021), p. 023236. DOI: 10.1103/PhysRevResearch.3.023236. URL: <https://link.aps.org/doi/10.1103/PhysRevResearch.3.023236>.
- [22] Wilhelm Kadow, Frank Pollmann and Michael Knap. ‘Isometric tensor network representations of two-dimensional thermal states’. In: *Phys. Rev. B* 107 (20 May 2023), p. 205106. DOI: 10.1103/PhysRevB.107.205106. URL: <https://link.aps.org/doi/10.1103/PhysRevB.107.205106>.
- [23] P.-A. Absil, R. Mahony and Rodolphe Sepulchre. *Optimization Algorithms on Matrix Manifolds*. Princeton: Princeton University Press, 2008. ISBN: 9781400830244. DOI: doi:10.1515/9781400830244. URL: <https://doi.org/10.1515/9781400830244>.
- [24] Ilia A Luchnikov, Mikhail E Krechetov and Sergey N Filippov. ‘Riemannian geometry and automatic differentiation for optimization problems of quantum physics and quantum technologies’. In: *New Journal of Physics* 23.7 (July 2021), p. 073006. ISSN: 1367-2630. DOI: 10.1088/1367-2630/ac0b02. URL: <http://dx.doi.org/10.1088/1367-2630/ac0b02>.
- [25] Markus Hauru, Maarten Van Damme and Jutho Haegeman. ‘Riemannian optimization of isometric tensor networks’. In: *SciPost Physics* 10.2 (Feb. 2021). ISSN: 2542-4653. DOI: 10.21468/scipostphys.10.2.040. URL: <http://dx.doi.org/10.21468/SciPostPhys.10.2.040>.
- [26] James Townsend, Niklas Koep and Sebastian Weichwald. *Pymanopt: A Python Toolbox for Optimization on Manifolds using Automatic Differentiation*. 2016. arXiv: 1603.03236 [cs.MS].